

Reduced graphene oxide modified activated carbon for improving power generation of air-cathode microbial fuel cells

Yang Yang

Key Laboratory of Low-Grade Energy Utilization Technologies and Systems, Institute of Engineering Thermophysics, Chongqing University, Chongqing 400030, People's Republic of China; Ministry of Education Key Laboratory of Micro/Nano Systems for Aerospace, School of Mechanical Engineering, Northwestern Polytechnical University, Xi'an 710072, People's Republic of China; and Department of Chemistry and Biochemistry, University of California, Santa Cruz, California 95060, USA

Tianyu Liu and Hanyu Wang

Department of Chemistry and Biochemistry, University of California, Santa Cruz, California 95060, USA

Xun Zhu,^{a)} Dingding Ye, and Qiang Liao

Key Laboratory of Low-Grade Energy Utilization Technologies and Systems, Institute of Engineering Thermophysics, Chongqing University, Chongqing 400030, People's Republic of China

Ke Liu, Shaowei Chen, and Yat Li^{b)}

Department of Chemistry and Biochemistry, University of California, Santa Cruz, California 95060, USA

(Received 9 June 2017; accepted 29 June 2017)

Activated carbon (AC) has been widely used as catalyst for oxygen reduction reaction (ORR) in air-cathode microbial fuel cells (MFCs). Here we demonstrate a new method to improve the AC air-cathode by blending it with reduced graphene oxide (rGO). rGO sheets are first deposited on Ni foam and AC is then brushed onto it with controlled mass loading. rGO sheets not only improve the electrical conductivity of AC, but also provide a large number of ORR areas. Rotating ring disk electrode measurements reveal that the number of transferred electrons at rGO-AC cathode is 3.5, indicating the four-electron pathway is the dominant process. Significantly, the MFC with rGO-AC cathode delivers a maximum power density of $2.25 \pm 0.05 \text{ W/m}^2$, which is substantially higher than that of plain AC cathode ($1.35 \pm 0.07 \text{ W/m}^2$) and those for other air-cathode MFCs using AC as ORR catalyst under the same mass loading.

I. INTRODUCTION

Air-cathode microbial fuel cells (MFCs) can recover wasted energy that is stored in organic matters in wastewater for generation of bioelectricity, and represent a promising solution for energy sustainability.^{1–6} Yet, noble metal catalysts such as platinum nanoparticles (Pt NPs) and Pt-based metal alloys are typically required to promote the oxygen reduction reaction (ORR) occurred at cathode.⁷ These noble metal catalysts are expensive and often suffer from time-dependent drift and CO deactivation,^{8,9} which limit the scalability and practicality of MFCs.¹⁰

Enormous efforts have been devoted to develop alternatives to Pt-based catalysts for MFCs.^{11–13} For example, nonprecious metal NPs, such as metal oxides¹⁴ and transition metal macrocyclic compounds¹⁵ have been studied for ORR. Khilari et al. reported the use of manganese cobaltite (MnCo_2O_4) nanorods and

polypyrrole (PPy) as an ORR composite catalyst.¹⁶ The MFC equipped with this *in situ*-synthesized composite achieved a maximum volumetric power density of 6.11 W/m^3 . Recently, low cost carbon materials, such as activated carbon (AC),¹⁷ AC nanofiber,¹⁸ carbon nanotube,^{19,20} and polypyrrole/carbon black composite²¹ have attracted a lot of attention. Among them, AC-based catalysts are particularly promising because of their outstanding electrochemical stability and cost effectiveness.^{17,22–25} In a previous study, the AC catalyst showed an excellent catalytic performance for ORR in MFCs, and was even comparable to the performance of Pt/C catalyst during a long-term operation. AC was cold-pressed with polytetrafluoroethylene (PTFE) as a binder onto a piece of Ni mesh at 150 bar. The maximum power density of 1220 mW/m^2 was obtained for MFCs with this AC air-cathode.²¹

However, the catalytic performance of AC is still limited by its poor electrical conductivity and relatively small number of ORR catalytic areas.²⁶ A number of approaches have been demonstrated to improve the catalytic performance of AC, such as adding the nitrogen-containing functional groups,^{22,23} pyrolyzing AC by iron ethylenediaminetetraacetic acid,²⁴ tailoring

Contributing Editor: Teng Zhai

Address all correspondence to these authors.

^{a)}e-mail: zhuxun@cqu.edu.cn

^{b)}e-mail: yatli@ucsc.edu

DOI: 10.1557/jmr.2017.283

the electrical conductivity by blending carbon black²⁶ and using metal meshes as current collectors.²⁵ These methods have been primarily focused on increasing the number of ORR active areas by adding other functional groups or improving the electrical conductivity. Nevertheless, the catalytic performance of the previously reported AC catalysts still has not satisfied the need for large-scale MFCs.²⁷ It is highly desirable to develop a new method for improving the catalytic performance of AC.

Here we reported a new design of air-cathode involving a three dimensional (3D) reduced graphene oxide (rGO) scaffold coated with AC (denoted as rGO-AC). The incorporation of graphene sheets enlarged the electrode surface area and provided more active areas for ORR.²⁸ The MFC device with this rGO-AC air-cathode achieved an outstanding power density of $2.25 \pm 0.05 \text{ W/m}^2$, which was substantially higher than the values reported for MFC devices with plain AC air-cathodes.^{25,26,29,30}

II. EXPERIMENTAL

A. Fabrication of rGO-AC air-cathode

The fabrication process of rGO-AC air-cathode is illustrated in Figs. 1(a)–1(c). Graphene oxide (GO) solution was first prepared according to a method published elsewhere.³¹ The concentration of GO solution was $\sim 1 \text{ mg/mL}$. A plain Ni foam substrate [Fig. 1(a)] was placed into a 25 mL autoclave with Teflon liner and filled with the GO solution. The autoclave was heated at $120 \text{ }^\circ\text{C}$ for 5 h and then cooled down at room temperature. Ni foam was removed from the autoclave, washed with de-ionized (DI) water and then air dried. The Ni foam was uniformly covered by graphene after repeating the above deposition process three times [Fig. 1(b)]. AC catalysts were deposited onto the rGO coated Ni foam using brushing method.³² Briefly, 1 g AC and 5 g Nafion solutions (5 wt%) were mixed with 56 mL ethanol in a beaker. Then the solution mixture was sonicated for 15 min to form a paste. The paste was brushed on one side of cathode and dried at $80 \text{ }^\circ\text{C}$ in an oven. The AC loading (14, 28, 35, 42 mg/cm^2) was controlled by varying the number of brushing process [Fig. 1(c)]. To facilitate oxygen diffusion, the other side of cathode was coated with four diffusion layers of hydrophobic PTFE using a previously reported method.³³ The working principle of rGO-AC air-cathodes is illustrated in Fig. 1(d). The electrons and protons are generated from the decomposition of organic matters via bacterial metabolism at anode. Oxygen (from air) can diffuse into the porous cathode and react with electrons and protons to form water (four-electron pathway) or hydrogen peroxide (two-electron pathway). A previous study found that the optimal loading of AC was $\sim 42 \text{ mg/cm}^2$.³⁴ Therefore, we prepared a control

cathode with AC ($\sim 42 \text{ mg/cm}^2$) deposited on a plain Ni foam for comparison.

B. Electrochemical characterizations

Electrochemical analyses, including chronoamperometry (CA), Tafel test and rotating ring disk electrode (RRDE) test, were carried out with a CHI 660D electrochemical station (Chenhua Instruments, Shanghai, China). Both CA and Tafel plots were collected in a three-electrode electrolytic cell with 50 mM phosphate buffer solution (PBS) as electrolyte. Air-cathodes were used as working electrodes with the oxygen diffusion layer facing the air. An Ag/AgCl electrode (saturated KCl, $+0.197 \text{ V}$ versus SHE) and a Pt plate (99.99%, 1 cm^2) were used as reference and counter electrode, respectively.

In CA measurements, the reactor was first operated in an open circuit mode to reach a stable state, and then applied by different voltages (0.2, 0.1, 0, -0.1 , -0.2 V) in a stepwise manner. In Tafel test, overpotential from 0 to 0.1 V was measured at a sweep rate of 1 mV/s . The value of exchange current density (j_0) can be obtained from Tafel equation [Eq. (1)] according to the intercept of y -axis:

$$\log|j| = \log j_0 + (\beta n F / 2.303 RT) |\eta| \quad (1)$$

where j is the measured current density, j_0 exchange current density, β electron transfer coefficient for reductive reaction, n number of electrons transferred, F Faraday's constant, R gas constant, T temperature, and η ORR overpotential. For RRDE tests, rotating (Pt) ring-(glassy-carbon) disk electrode was selected as the working electrode. Catalyst ink was prepared by mixing 0.4 mg catalyst powder (plain AC, or rGO-AC powder) and 1.6 mg carbon black (XC-72) with $4 \text{ } \mu\text{L}$ Nafion solutions, followed by ultrasonic mixing with 0.4 mL ethanol. $20 \text{ } \mu\text{L}$ catalyst inks were added drop wise onto the ring disk electrode and dried under nitrogen atmosphere. Before RRDE measurement, $3 \text{ } \mu\text{L}$ 2 wt% Nafion solutions were added to samples as extra binders.

C. Material characterization

The scanning electron microscope (SEM) images of air-cathode materials were collected by a field-emission SEM (Hitachi S4800 II, Hitachi, Tokyo, Japan). The specific surface areas of plain AC and rGO-AC were identified by surface area and porosimetry analyzer (ASAP 2020, Micromeritics, Norcross, Georgia). The Brunauer–Emmett–Teller (BET) measurements were performed using nitrogen adsorption and desorption isotherms at 77.3 K . Pore width–volume plots were analyzed according to the density functional theory (DFT). To further identify the electrochemical active surface area, cyclic voltammograms at different scan rates were collected and reciprocal of areal capacitance

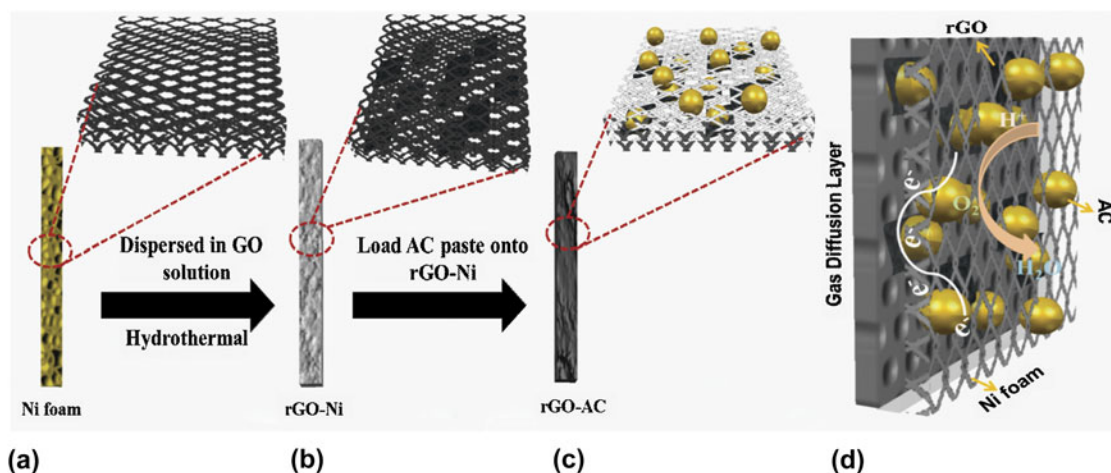


FIG. 1. (a–c) Schematic illustration of the fabrication process of rGO-AC cathode. Ni foam was hydrothermally treated in GO solution to obtain rGO-coated Ni foam. AC, Nafion, and ethanol were mixed at a ratio 9:4:1 to form a paste, which was brushed onto the rGO-coated Ni foam. (d) Schematic diagram of rGO-AC cathode.

($1/C$) against square root of scan rate ($v^{1/2}$) were plotted as previously mentioned.³⁵

D. MFC setup

A 28 mL single-chamber MFC device was constructed via the assembly of 3D rGO-coated Ni foam anode (denoted as rGO-Ni)³¹ and rGO-AC (or plain AC) coated Ni foam cathode. All MFCs were inoculated from the culture enriched with *Shewanella oneidensis* MR-1 (ATCC-700550, ATCC, Manassas, Virginia). Bacteria were cultured in an incubator shaker contained 30 g/L trypticase soy broth (TSB, BD Biosciences, San Jose, CA) medium with shaking at 150 rpm at a constant temperature (30 ± 1 °C).³¹ To maintain the bacterial metabolism environment neutral (pH value ~ 7.0), the nutrient were further diluted in 50 mM PBS that contained 9.1 g/L K_2HPO_4 and 1.28 g/L KH_2PO_4 .³¹ MFCs were inoculated under the external resistance of 500 Ω and voltage (U) was recorded using a data acquisition system (2700 Keithley, Keithley Instruments, Solon, Ohio) every 10 s. Once the voltage dropped to the baseline, i.e., 50 mV, reactors were refreshed by adding fresh TSB medium.

Cell performance was tested after successful inoculation by varying the external resistance (R) from 3900 to 10 Ω . Current (I) was calculated according to the ohm's law: $I = U/R$ and power (P) was calculated based on the equation: $P = U \times I$. Both the current density and power density were normalized to the electrode surface area (~ 5 cm²). All MFC measurements were repeated three times to ensure good reproducibility.

The electrochemical impedance spectroscopy (EIS) was carried out in a two-electrode configuration at a constant voltage of 0.1 V over a frequency range of 10,000–0.01 Hz with a perturbation of 10 mV. EIS data was analyzed using *ZSimpwin* software (Princeton

Applied Research, Berwyn, Pennsylvania) by fitting the spectra with an equivalent electric circuit.

III. RESULTS AND DISCUSSION

A. Structural analyses of rGO-AC catalysts

The structures of plain Ni and AC-loaded Ni foams were characterized by SEM. The plain Ni foam showed a smooth surface [Fig. 2(a)]. Upon refluxing in rGO solution, the Ni foam was gradually covered by graphene sheets [Fig. 2(b)]. Then, rGO-AC electrodes with different AC loadings were prepared by controlled variation of the number of loading cycles [Figs. 2(c)–2(f)]. By repeating the loading process, the thickness and roughness of the air-cathodes increased with AC loading. Meanwhile, some of the pores were blocked when large amount of AC (42 mg/cm²) were coated on the scaffold [Fig. 2(f)]. The blockage of pores may affect the oxygen diffusion efficiency and limit the catalytic performance.³⁶

N_2 adsorption/desorption measurements were performed to investigate the specific surface area and pore distribution of these electrodes. The pore-diameter detection range of this measurement is from 0.35 to 500 nm. Fig. S1(a) shows the type-IV curves of isotherms obtained from these samples that are consistent with the curves reported for AC-based catalysts.^{37,38} Pore characteristics of different catalysts are summarized in Table S1. The rGO-AC sample with the highest AC loading (42 mg/cm²) exhibited the largest BET specific surface area of 313.41 m²/g, which was almost 2-folds higher than that of the plain AC (157.81 m²/g). Nevertheless the macro-pores (pore size \sim hundreds of micrometers) began to be blocked with increasing the mass loading of AC, rGO-AC sample with the highest loading (42 mg/cm²) still exhibited the largest specific surface area. One

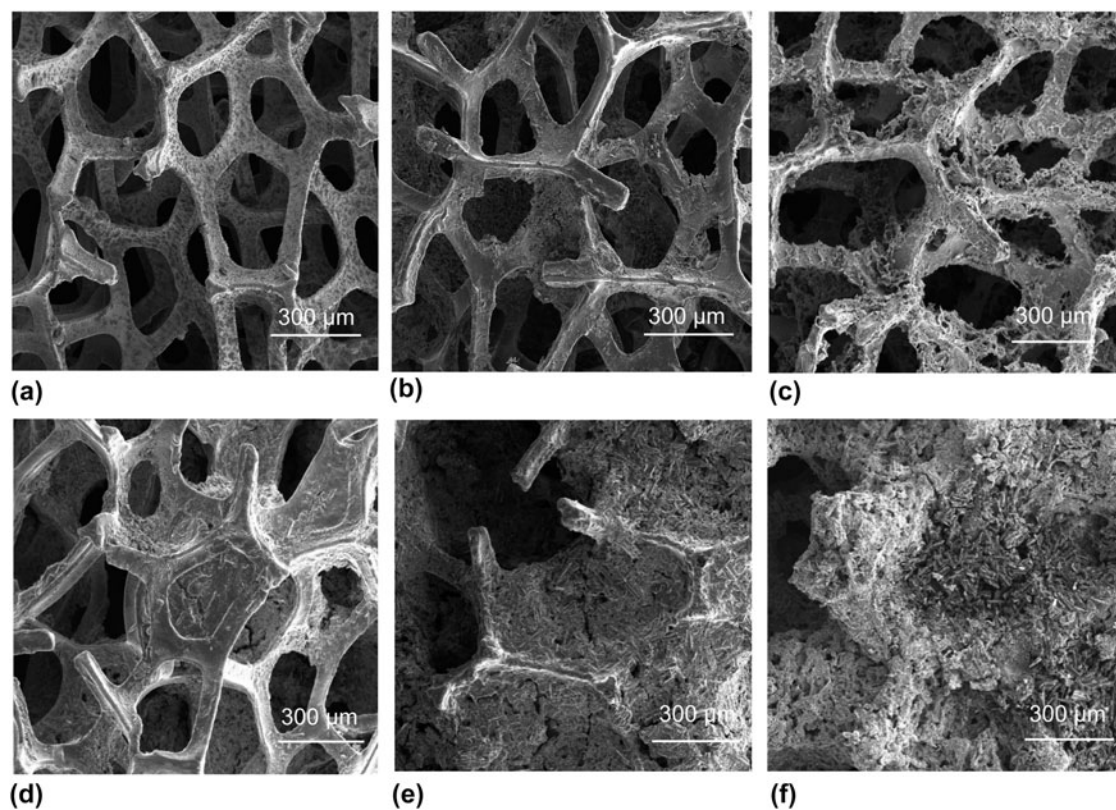


FIG. 2. SEM images showing the surface morphology of (a) plain Ni foam; (b) rGO-Ni (no AC); (c–f) rGO-AC (14, 28, 35, 42 mg/cm²).

side, the largest BET surface area is related to the increased amount of micro-pores from AC. On the other side, it is believed to be contributed from graphene sheets, which have a high theoretical surface area of 2630 m²/g.³⁹

In the plot of pore diameter as a function of incremental pore volume [Fig. S1(b)], all rGO-AC catalysts exhibited a peak centered at around 2.5 nm, while this peak was not observed for plain AC. The average pore diameter was drastically decreased from 18.22 to 3.22 nm with the increasing amount of AC (Table S1). It confirms that the amount of micro-pores gradually increases after blending the AC with graphene sheets. The high ratio of micro-/meso-pores in AC catalysts is favorable for ORR and can further boost catalytic activity.³⁷ Meanwhile, the broad distribution of pore diameters can also facilitate the ion transport and charge transfer during ORR.

B. MFC performance

The performance of MFCs equipped with these rGO-AC air-cathodes was tested in a single-chamber device [Fig. 3(a)]. Three-dimensional rGO-Ni was used as the bio-anode. After repeating the inoculation process for three cycles in a batch-mode, *S. oneidensis* MR-1 cells were successfully colonized on the electrodes and formed a compact biofilm as the SEM image indicated [Fig. 3(b)].

The dense bacterial film on the anodic surface ensures stable performance of bio-catalyzed reactions on the bio-anode side. Figure 4 shows the power density and polarization curves collected from different cathodes. Among them, the MFC with rGO-AC (35 mg/cm²) cathode achieved the best performance with the highest maximum power density of 2.25 ± 0.05 W/m² at a current density of 6.70 ± 0.07 A/m², which was 66.7% higher than that of plain AC cathode (1.35 ± 0.07 W/m²). When the MFCs were connected to a resistor of 10 Ω, the rGO-AC (35 mg/cm²) MFC generated the highest current density of 13.1 ± 0.45 A/m². In the polarization curves shown in Fig. 4(b), MFC with rGO-AC (35 mg/cm²) cathode also exhibited the highest open circuit voltage (OCV, 0.63 ± 0.03 V) among all devices. Since all the tested MFCs have identical bio-anodes, the difference in cell device performance should be ascribed to the different performance of the cathodes (Fig. S2).

To understand the role of rGO, we compared the cyclic voltammograms (CV) of rGO-AC (35 mg/cm²) and AC. As shown in Fig. S3, rGO-AC exhibits a quasirectangular shape of CV, while the CV of plain AC is highly distorted. The results suggest that rGO-AC has a smaller internal resistance. Nyquist plots were also collected to further determine the resistances of MFCs with different cathodes. All data were collected at a constant external voltage of 0.1 V, and fitted by an equivalent electric circuit shown in Fig. S4. Table I summarizes the EIS

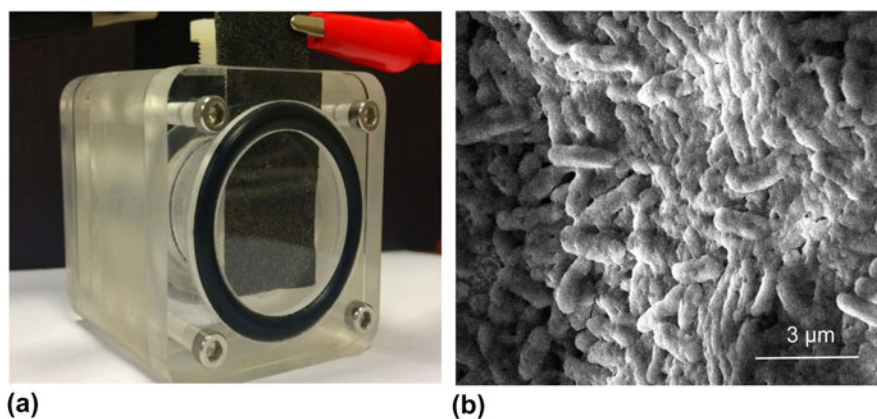


FIG. 3. (a) Schematic diagram illustrating the configuration of a single-chamber MFC device. MR-1/TSB solution was used as anolyte; (b) SEM image of anodic surface covered by *S. oneidensis* MR-1 cells. The scale bar is 3 μm .

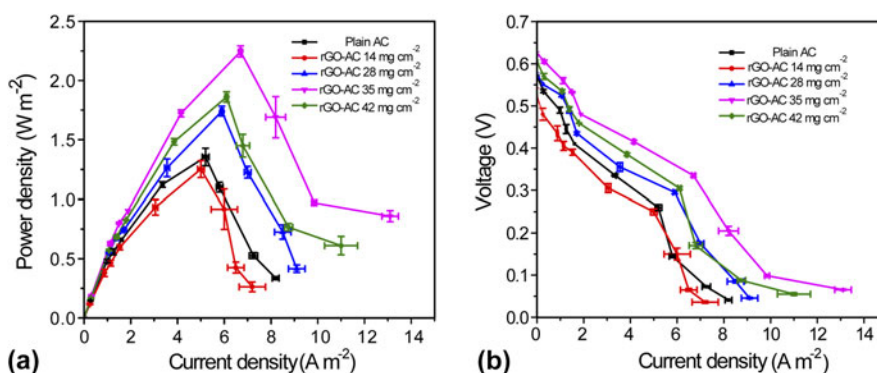


FIG. 4. Plots of (a) power density and (b) voltage as a function of current density of MFCs with different air-cathodes. Error bars represent the standard deviations evaluated based on data collected in triplicate.

TABLE I. EIS fitting results of MFCs with different air-cathodes.

	Ohmic resistance/ Ω	Charge transfer resistance/ Ω	Diffusion resistance/ Ω	Whole cell resistance/ Ω
Plain AC	26.53	519.38	86.72	632.63
rGO-AC 14 mg/cm ²	17.05	23.86	63.84	104.75
rGO-AC 28 mg/cm ²	11.19	3.52	40.94	66.75
rGO-AC 35 mg/cm ² (premium sample)	9.45	0.39	32.36	42.20
rGO-AC 42 mg/cm ²	10.46	47.31	43.09	100.86

fitting results. As shown in Fig. 5, MFCs with rGO-AC cathodes have considerably smaller semicircles in the middle frequency domain compared to the MFC with a plain AC cathode, suggesting these cathodes have smaller charge transfer resistances.^{17,26} The rGO-AC (35 mg/cm²) sample exhibited the smallest charge transfer resistance (0.39 Ω) and internal resistance (42.2 Ω), which are orders of magnitude smaller than that of plain AC (charge transfer resistance of 519.38 Ω and internal resistance of 650 Ω). The reduced charge transfer resistance can be attributed to the presence of highly conductive rGO sheets that facilitates charge transfer. Notably, rGO-AC (35 mg/cm²) MFC also has the smallest resistances among the rGO-AC MFCs. The results

indicate that 35 mg/cm² is an optimal AC loading for the rGO-coated Ni foam used in this study. The increased resistance observed for rGO-AC (42 mg/cm²) MFC is believed to be due to the excess AC loading that blocks the pores, as shown in Fig. 2(f).

C. Electrochemical performance of rGO-AC cathodes

To further investigate the electrochemical properties of different air-cathodes, current–potential curves were collected in a home built electrochemical reactor. As shown in Fig. 6(a), rGO-AC (42 mg/cm²) achieved a current density of 12.7 A/m² at 0.2 V versus Ag/AgCl, which was substantially higher than that of plain AC (8.8 A/m²)

with the same mass loading. The result again confirmed that the electro-catalytic activity of AC was enhanced by mixing with rGO sheets. Furthermore, the exchange current density (j_0) of these cathodes was evaluated by a Tafel test performed in 50 mM PBS (Fig. S5). Exchange current is the current density of working electrode when over-potential is zero. It relates to the electrochemical activity of the electrode at equilibrium state. j_0 was calculated according to the Tafel equation [Eq. (1)] using the data in the linear region (overpotential

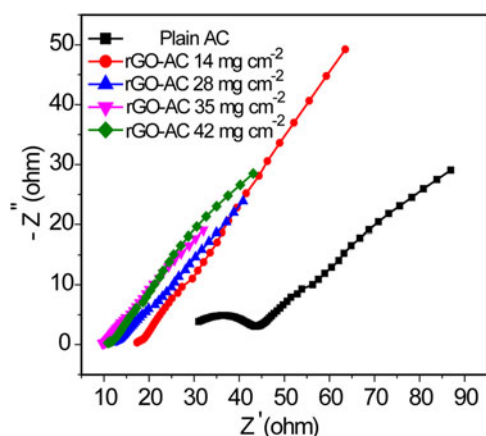


FIG. 5. Nyquist plots of MFCs with various rGO-AC catalysts under an external voltage of 0.1 V. Frequency range: 10,000–0.01 Hz.

ranged from 80 to 100 mV, inset of Fig. S5). As shown in Fig. S5, rGO-AC (42 mg/cm^2) achieved the maximum j_0 of $2.23 \times 10^{-4} \text{ A/cm}^2$, which was two times higher than that of plain AC ($0.93 \times 10^{-4} \text{ A/cm}^2$) with the same mass loading. More importantly, the j_0 of rGO-AC is considerably higher than the values reported for other AC-based cathodes.^{37,38} The enhanced current density can be attributed to the increased ORR activity as a result of the well-distributed micro-pores of graphene sheets.

D. Catalysis kinetics

To understand the catalytic properties of AC and rGO-AC for ORR, RRDE technique was carried out to quantitatively characterize the ORR electron transfer pathway for plain AC and rGO-AC with optimal loading (35 mg/cm^2). As shown in Figs. 6(b) and 6(c), the cathodic currents were measured in the potential range between -0.32 V and $+0.67 \text{ V}$ under different rotating speeds (100, 400, 900, 1600, 2500 rpm). Both catalysts have the same onset potential of $+0.35 \text{ V}$ versus Ag/AgCl. However, the disk currents generated by rGO-AC at different rotating speeds are considerably larger than the values obtained from plain AC [Fig. 6(c)], indicating improved ORR efficiency on rGO-AC electrode related to number of transferred electrons.^{40,41} Meanwhile, the ring currents were about one order of magnitude smaller than the disk currents under the same potentials. It indicated that peroxide species were rarely

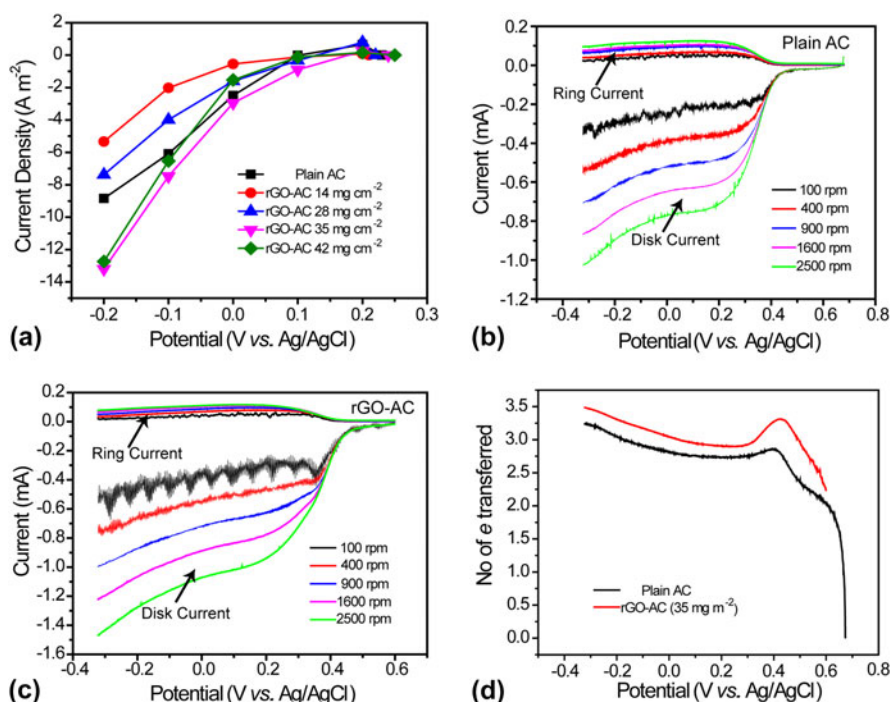


FIG. 6. (a) Current–potential curves of plain AC and rGO-AC cathodes collected in 50 mM PBS solution; RRDE voltammograms of catalyst inks of (b) plain AC and (c) rGO-AC 35 mg/cm^2 in an oxygen-saturated 0.1 M KOH solution; (d) A plot of number of transferred electrons calculated from the RRDE voltammograms at 1600 rpm.

TABLE II. Comparison of MFC device performance of using different AC air-cathodes.

Anode material	Cathode catalyst	Bacteria	Anode chamber volume (mL)	Maximum power density (W/m ²)	Maximum current density (A/m ²)	References
Graphite fiber brush	AC by blending carbon black	...	26	1.56	10.0	26
Carbon mesh	Ultra-capacitor AC	Mixed bacteria	28	1.4	6	25
Graphite fiber brush	AC	Mixed bacteria	28	1.21	~7.5	17
Carbon mesh	Rolling AC with PTFE	Mixed bacteria	28	0.802	~4	38
Carbon mesh	Rolling non-sintered AC	Mixed bacteria	28	1.086	~5	48
Stainless steel mesh	Alkaline pretreatment AC	Mixed bacteria	28	0.957	4.2	49
Carbon paper	AC + Pt/Pd	Mixed bacteria	28	1.42	7	30
rGO-Ni	AC by blending rGO	Shewanella MR-1	28	2.25 ± 0.05	13.1 ± 0.45	This work

generated during the ORR process. Under the low rotating speeds (e.g., 100, 400 rpm), a fluctuation was observed as a result of a relative slow diffusion rate of oxygen to the electrode. To avoid the issue of diffusion-rate limitation, further details in the ORR process were analyzed at high rotating speed approached 900 rpm and beyond. For example, the number of transferred electrons (n) was estimated based on the following equation at 1600 rpm [Eq. (2)]:⁴²

$$n = \frac{4I_D}{(I_D + \frac{I_R}{N})} \quad (2)$$

where I_R is the ring current, I_D the disk current, and N the collection efficiency (37%). n increased dramatically from 0 to 3.0 when the potential changed from 0.67 to 0.4 V [Fig. 6(d)]. It is suggested that four-electron water oxidation was the dominant process on AC-species catalysts, in which O_2 was mainly converted to OH^- rather than HO_2^- . When potential was further increased, n gradually increased to 3.5 for rGO-AC, which was higher than that of plain AC ($n = 3.2$). The yield of peroxide was calculated by Eq. (3):^{43,44}

$$\%(\text{HO}_2^-) = 200 \times \frac{I_R/N}{(I_D + I_R/N)} \quad (3)$$

The yield of peroxide for rGO-AC catalyst was calculated to be 25.5% at stable catalysis, which was substantially lower than the value of plain AC (38.9%). The results are consistent with the conclusion that the charge transfer efficiency of AC was enhanced by blending it with rGO sheets. The positive role of rGO sheets is believed to be due to its contributions of large specific surface area and abundant micro-/meso-pores,

which can increase the number of oxygen reduction areas and facilitate ion transfer.^{36,37} Notably, the ion-accessible surface area of rGO-AC estimated by Trasatti method (Fig. S6)^{45,46} is comparable to the value obtained from BET measurements, again proving the unique rGO structure can facilitate electrolyte/ion diffusion.

IV. CONCLUSIONS

In summary, we have successfully synthesized a new ORR catalyst for MFC cathode by mixing AC with rGO sheets. Table II summarizes the performance of some recently reported MFCs with AC-based air-cathodes and compares to the MFC performance with rGO-AC as catalysts. MFC with rGO-AC (35 mg/cm²) produces a maximum power density of 2.25 ± 0.05 W/m², which is the highest value obtained from air-cathode MFCs inoculated with pure strain of *S. oneidensis* MR-1 in a similar size reactor. The new rGO-AC catalyst in terms of cost (~\$2 per gram⁴⁷) should be potentially affordable for large scale MFC systems.

ACKNOWLEDGMENTS

This work is supported by the National Natural Science Funds for Distinguished Young Scholar (No. 51325602), International Cooperation and Exchange of the National Natural Science Foundation of China (No. 51620105011), National Natural Science Foundation of China (No. 51376203). Y.L. thanks the financial support from NSF (IIP-1550327). Y.Y. thanks the China Scholarship Council for financial support and the Fundamental Research Funds for the Central Universities (3102017OQD011).

REFERENCES

1. B.E. Logan: Exoelectrogenic bacteria that power microbial fuel cells. *Nat. Rev. Microbiol.* **7**, 375 (2009).
2. D.R. Lovley: The microbe electric: Conversion of organic matter to electricity. *Curr. Opin. Biotechnol.* **19**, 564 (2008).
3. W-W. Li, H-Q. Yu, and Z. He: Towards sustainable wastewater treatment by using microbial fuel cells-centered technologies. *Energ. Environ. Sci.* **7**, 911 (2014).
4. W. Yang, J. Li, D. Ye, X. Zhu, and Q. Liao: Bamboo charcoal as a cost-effective catalyst for an air-cathode of microbial fuel cells. *Electrochim. Acta* **224**, 585 (2017).
5. C. Haixing, F. Qian, H. Yun, X. Ao, L. Qiang, and Z. Xun: Improvement of microalgae lipid productivity and quality in an ion-exchange-membrane photobioreactor using real municipal wastewater. *Int. J. Agric. Biol. Eng.* **10**, 97 (2017).
6. H-X. Chang, Y. Huang, Q. Fu, Q. Liao, and X. Zhu: Kinetic characteristics and modeling of microalgae *Chlorella vulgaris* growth and CO₂ biofixation considering the coupled effects of light intensity and dissolved inorganic carbon. *Bioresour. Technol.* **206**, 231 (2016).
7. H. Rismani-Yazdi, S.M. Carver, A.D. Christy, and O.H. Tuovinen: Cathodic limitations in microbial fuel cells: An overview. *J. Power Sources* **180**, 683 (2008).
8. X. Yu and S. Ye: Recent advances in activity and durability enhancement of Pt/C catalytic cathode in PEMFC. *J. Power Sources* **172**, 145 (2007).
9. M. Winter and R.J. Brodd: What are batteries, fuel cells, and supercapacitors? *Chem. Rev.* **104**, 4245 (2004).
10. S. Bajracharya, A. ElMekawy, S. Srikanth, and D. Pant: 6-Cathodes for microbial fuel cells. In *Microbial Electrochemical and Fuel Cells*, K. Scott and E.H. Yu, ed. (Woodhead Publishing, Sawston, Cambridge, U.K., 2016); p. 179.
11. X.B. Gong, S.J. You, X.H. Wang, J.N. Zhang, Y. Gan, and N.Q. Ren: A novel stainless steel mesh/cobalt oxide hybrid electrode for efficient catalysis of oxygen reduction in a microbial fuel cell. *Biosens. Bioelectron.* **55**, 237 (2014).
12. G. Gnana Kumar, Z. Awan, K. Suk Nahm, and J.S. Xavier: Nanotubular MnO₂/graphene oxide composites for the application of open air-breathing cathode microbial fuel cells. *Biosens. Bioelectron.* **53**, 528 (2014).
13. J. Huang, N. Zhu, T. Yang, T. Zhang, P. Wu, and Z. Dang: Nickel oxide and carbon nanotube composite (NiO/CNT) as a novel cathode non-precious metal catalyst in microbial fuel cells. *Biosens. Bioelectron.* **72**, 332 (2015).
14. X.Y. Yan, X.L. Tong, Y.F. Zhang, X.D. Han, Y.Y. Wang, G.Q. Jin, Y. Qin, and X.Y. Guo: Cuprous oxide nanoparticles dispersed on reduced graphene oxide as an efficient electrocatalyst for oxygen reduction reaction. *Chem. Commun.* **48**, 1892 (2012).
15. S. Guo, S. Zhang, L. Wu, and S. Sun: Co/CoO nanoparticles assembled on graphene for electrochemical reduction of oxygen. *Angew. Chem.* **51**, 11770 (2012).
16. S. Khilari, S. Pandit, D. Das, and D. Pradhan: Manganese cobaltite/polypyrrole nanocomposite-based air-cathode for sustainable power generation in the single-chambered microbial fuel cells. *Biosens. Bioelectron.* **54**, 534 (2014).
17. F. Zhang, D. Pant, and B.E. Logan: Long-term performance of activated carbon air cathodes with different diffusion layer porosities in microbial fuel cells. *Biosens. Bioelectron.* **30**, 49 (2011).
18. M. Ghasemi, S. Shahgaldi, M. Ismail, B.H. Kim, Z. Yaakob, and W.R.W. Daud: Activated carbon nanofibers as an alternative cathode catalyst to platinum in a two-chamber microbial fuel cell. *Int. J. Hydrogen Energy* **36**, 13746 (2011).
19. K. Gong, F. Du, Z. Xia, M. Durstock, and L. Dai: Nitrogen-doped carbon nanotube arrays with high electrocatalytic activity for oxygen reduction. *Science* **323**, 760 (2009).
20. L. Feng, Y. Yan, Y. Chen, and L. Wang: Nitrogen-doped carbon nanotubes as efficient and durable metal-free cathodic catalysts for oxygen reduction in microbial fuel cells. *Energ. Environ. Sci.* **4**, 1892 (2011).
21. Y. Yuan, S. Zhou, and L. Zhuang: Polypyrrole/carbon black composite as a novel oxygen reduction catalyst for microbial fuel cells. *J. Power Sources* **195**, 3490 (2010).
22. B. Zhang, Z. Wen, S. Ci, S. Mao, J. Chen, and Z. He: Synthesizing nitrogen-doped activated carbon and probing its active sites for oxygen reduction reaction in microbial fuel cells. *ACS Appl. Mater. Interfaces* **6**, 7464 (2014).
23. V.J. Watson, C.N. Delgado, and B.E. Logan: Improvement of activated carbons as oxygen reduction catalysts in neutral solutions by ammonia gas treatment and their performance in microbial fuel cells. *J. Power Sources* **242**, 756 (2013).
24. X. Xia, F. Zhang, X. Zhang, P. Liang, X. Huang, and B.E. Logan: Use of pyrolyzed iron ethylenediaminetetraacetic acid modified activated carbon as air-cathode catalyst in microbial fuel cells. *ACS Appl. Mater. Interfaces* **5**, 7862 (2013).
25. S. Cheng and J. Wu: Air-cathode preparation with activated carbon as catalyst, PTFE as binder and nickel foam as current collector for microbial fuel cells. *Bioelectrochemistry* **92**, 22 (2013).
26. X. Zhang, X. Xia, I. Ivanov, X. Huang, and B.E. Logan: Enhanced activated carbon cathode performance for microbial fuel cell by blending carbon black. *Environ. Sci. Technol.* **48**, 2075 (2014).
27. Y. Alvarez-Gallego, X. Dominguez-Benetton, D. Pant, L. Diels, K. Vanbroekhoven, I. Genné, and P. Vermeiren: Development of gas diffusion electrodes for cogeneration of chemicals and electricity. *Electrochim. Acta* **82**, 415 (2012).
28. C. Zhu and S. Dong: Recent progress in graphene-based nano-materials as advanced electrocatalysts towards oxygen reduction reaction. *Nanoscale* **5**, 1753 (2013).
29. L. Qu, Y. Liu, J-B. Baek, and L. Dai: Nitrogen-doped graphene as efficient metal-free electrocatalyst for oxygen reduction in fuel cells. *ACS Nano* **4**, 1321 (2010).
30. F. Zhang, S. Cheng, D. Pant, G.V. Bogaert, and B.E. Logan: Power generation using an activated carbon and metal mesh cathode in a microbial fuel cell. *Electrochem. Commun.* **11**, 2177 (2009).
31. H. Wang, G. Wang, Y. Ling, F. Qian, Y. Song, X. Lu, S. Chen, Y. Tong, and Y. Li: High power density microbial fuel cell with flexible 3D graphene-nickel foam as anode. *Nanoscale* **5**, 10283 (2013).
32. S. Cheng, H. Liu, and B.E. Logan: Increased performance of single-chamber microbial fuel cells using an improved cathode structure. *Electrochem. Commun.* **8**, 489 (2006).
33. H. Liu and B.E. Logan: Electricity generation using an air-cathode single chamber microbial fuel cell in the presence and absence of a proton exchange membrane. *Environ. Sci. Technol.* **38**, 4040 (2004).
34. B. Wei, J.C. Tokash, G. Chen, M.A. Hickner, and B.E. Logan: Development and evaluation of carbon and binder loading in low-cost activated carbon cathodes for air-cathode microbial fuel cells. *RSC Adv.* **2**, 12751 (2012).
35. M. Sharma, S. Bajracharya, S. Gildemyn, S.A. Patil, Y. Alvarez-Gallego, D. Pant, K. Rabaey, and X. Dominguez-Benetton: A critical revisit of the key parameters used to describe microbial electrochemical systems. *Electrochim. Acta* **140**, 191 (2014).
36. X. Ren, S.S. Zhang, D.T. Tran, and J. Read: Oxygen reduction reaction catalyst on lithium/air battery discharge performance. *J. Mater. Chem.* **21**, 10118 (2011).

37. H. Dong, H. Yu, and X. Wang: Catalysis kinetics and porous analysis of rolling activated carbon-PTFE air-cathode in microbial fuel cells. *Environ. Sci. Technol.* **46**, 13009 (2012).
38. H. Dong, H. Yu, X. Wang, Q. Zhou, and J. Feng: A novel structure of scalable air-cathode without Nafion and Pt by rolling activated carbon and PTFE as catalyst layer in microbial fuel cells. *Water Res.* **46**, 5777 (2012).
39. X. Zhu, Y. Zhu, S. Murali, M.D. Stoller, and R.S. Ruoff: Nanostructured reduced graphene oxide/Fe₂O₃ composite as a high-performance anode material for lithium ion batteries. *ACS Nano* **5**, 3333 (2011).
40. Y. Garsany, O.A. Baturina, K.E. Swider-Lyons, and S.S. Kocha: Experimental methods for quantifying the activity of platinum electrocatalysts for the oxygen reduction reaction. *Anal. Chem.* **82**, 6321 (2010).
41. N.M. Markovic, H.A. Gasteiger, and P.N. Ross, Jr.: Oxygen reduction on platinum low-index single-crystal surfaces in sulfuric acid solution: Rotating ring-Pt (hkl) disk studies. *J. Phys. Chem.* **99**, 3411 (1995).
42. M. Lefèvre and J-P. Dodelet: Fe-based catalysts for the reduction of oxygen in polymer electrolyte membrane fuel cell conditions: Determination of the amount of peroxide released during electro-reduction and its influence on the stability of the catalysts. *Electrochim. Acta* **48**, 2749 (2003).
43. G. Wu, K.L. More, C.M. Johnston, and P. Zelenay: High-performance electrocatalysts for oxygen reduction derived from polyaniline, iron, and cobalt. *Science* **332**, 443 (2011).
44. Y. Liang, Y. Li, H. Wang, J. Zhou, J. Wang, T. Regier, and H. Dai: Co₃O₄ nanocrystals on graphene as a synergistic catalyst for oxygen reduction reaction. *Nat. Mater.* **10**, 780 (2011).
45. T. Liu, L. Finn, M. Yu, H. Wang, T. Zhai, X. Lu, Y. Tong, and Y. Li: Polyaniline and polypyrrole pseudocapacitor electrodes with excellent cycling stability. *Nano Lett.* **14**, 2522 (2014).
46. S. Ardizzzone, G. Fregonara, and S. Trasatti: "Inner" and "outer" active surface of RuO₂ electrodes. *Electrochim. Acta* **35**, 263 (1990).
47. X. Xie, G. Yu, N. Liu, Z. Bao, C.S. Criddle, and Y. Cui: Graphene-sponges as high-performance low-cost anodes for microbial fuel cells. *Energ. Environ. Sci.* **5**, 6862 (2012).
48. H. Dong, H. Yu, H. Yu, N. Gao, and X. Wang: Enhanced performance of activated carbon-polytetrafluoroethylene air-cathode by avoidance of sintering on catalyst layer in microbial fuel cells. *J. Power Sources* **232**, 132 (2013).
49. X. Wang, N. Gao, Q. Zhou, H. Dong, H. Yu, and Y. Feng: Acidic and alkaline pretreatments of activated carbon and their effects on the performance of air-cathodes in microbial fuel cells. *Bioresour. Technol.* **144**, 632 (2013).

Supplementary Material

To view supplementary material for this article, please visit <https://doi.org/10.1557/jmr.2017.283>.